ELSEVIER

Earth and Planetary Science Letters 151 (1997) 289–301

EPSL

The origin of sulfide-rimmed metal grains in ordinary chondrites

Dante S. Lauretta [a,b,*], Katharina Lodders [a,b], Bruce Fegley Jr. [a,b], Daniel T. Kremser [b]

[a] *Planetary Chemistry Laboratory, Campus Box 1169, Washington University, One Brookings Drive, St. Louis, MO 63130-4899, USA*
[b] *Department of Earth and Planetary Science, Campus Box 1169, Washington University, One Brookings Drive, St. Louis, MO 63130-4899, USA*

Received 25 October 1996; revised 27 May 1997; accepted 1 July 1997

Abstract

We report results from an experimental study of sulfide chemistry during metamorphism on ordinary chondrite parent bodies. Artificial LL-chondrite material, composed of silicate, iron metal, and sulfide grains, was placed in sealed, evacuated silica tubes and heated to either 500°C or 900°C. These temperatures are representative peak metamorphic temperatures experienced by type 3 and type 6 ordinary chondrites, respectively. Rapid sulfur mobilization occurs during heating and results in the formation of sulfide rims around the metal grains and sulfur loss from the original sulfide crystals. The newly formed sulfide rims have two distinct layers that incorporate nearby silicate grains. We also observe narrow sulfide trails that follow silicate grain boundaries and connect separate sulfide-rimmed metal grains. The morphologies of the sulfide rims suggest that vapor transport is the main mechanism for sulfur mobilization. Sulfur loss is observed along cracks and crystal boundaries of the initial sulfide grains. After extensive reaction, patches of iron metal appear at the outer edges of the sulfide crystals and large pore spaces form throughout the original sulfides. The experimental metal–sulfide assemblages resemble those found in low metamorphic grade ordinary chondrites. This suggests metamorphism is mainly responsible for the observed metal–sulfide textures in these chondrites. © 1997 Elsevier Science B.V.

Keywords: metals; troilite; pyrrhotite; ordinary chondrites; metamorphism

1. Introduction

Sulfur is predicted to condense in the solar nebula by the gas–solid reaction:

$$\mathrm{FeNi(metal)} + \mathrm{H_2S(g)} \rightarrow (\mathrm{Fe,Ni})_{1-x}\mathrm{S} + \mathrm{H_2(g)} \quad (1)$$

between metal and H_2S gas [1]. Previous experimental studies of the sulfurization of iron metal and iron–nickel alloys in H_2–H_2S gas mixtures show that the morphology, crystal orientation, and composition of the resulting sulfide layers vary with temperature and H_2S/H_2 ratio [1–3]. In addition, since sulfide growth is controlled by cation diffusion, Fe and Ni concentration gradients are present in the sulfide layers [1–3]. The magnitude of these concentration gradients is a function of the temperature and sulfur fugacity during sulfide formation. Thus, identification and analyses of pristine nebular sulfide condensates in chondrites could be a powerful tool for determining the conditions that prevailed in the early solar nebula during sulfide formation.

* Corresponding author. Tel.: +1 314 935 7595. Fax: +1 314 935 4853. E-mail: lauretta@wunder.wustl.edu

PII S0012-821X(97)00122-2

We looked for evidence of nebular sulfides by performing microscopic examination and electron microprobe analyses of the metal–sulfide assemblages in the unequilibrated ordinary chondrite Allan Hills 76004 (ALH-76004, LL3.2/3.4 breccia) [1]. We found no concentration gradients in these assemblages indicative of gas–solid reaction in the solar nebula. Instead, the morphology and bulk composition of these grains suggested that Fe, Ni, and S were redistributed during a post-accretion heating event on the LL-chondrite parent body [1]. This suggestion implies that sulfur was mobilized during low temperature metamorphism on the ordinary chondrite parent body. This idea is supported by observations of sulfur mobilization in a qualitative simulation of metamorphism in carbonaceous chondrites [4]. However, detailed information is lacking on sulfur transport mechanisms during low temperature metamorphism. Thus, we began a series of experiments to study sulfide chemistry during metamorphic events on LL-chondrite parent bodies.

2. Experimental procedure

The experimental charges consist of three components: silicates, high purity iron metal, and sulfide crystals. The silicate portion was prepared by fusing a mixture of components having the same normative mineralogy as the silicates in LL-chondrites [5]. The composition of each component and the bulk silicate mixture are given in Table 1. The well mixed silicate components were heated for 2 h at 1550°C to fuse the components together. The resulting silicate bead was crushed with an agate mortar and pestle yielding grain sizes ≤ 50 μm.

The iron used for the experiments was Fisher Chemical certified pure iron metal powder (99.5%) with an average grain size of ~ 50 μm. The sulfide crystals were produced by sulfurization of iron metal foil in an H_2–H_2S gas mixture containing 1% H_2S at 900°C [2,3], yielding an average Fe/S ratio of 0.976 and an average sulfide grain size of ~ 500 μm.

It is important to remember that troilite is the iron-rich end-member of the pyrrhotite solid solution series which extends from FeS to Fe_7S_8. Pyrrhotites with Fe/S greater than 0.98 have the troilite unit cell and are thus considered to be troilite [2,6]. However, any sulfide that forms by reaction between metal and S-bearing gas has a bulk Fe/S ratio less than unity and a compositional gradient that extends from an Fe-rich composition at the metal–sulfide interface to a S-rich one at the sulfide–gas interface. This gradient is a function of temperature, sulfur fugacity, and the reaction kinetics. Experimental studies of sulfide formation under nebular conditions produce sulfides ranging in composition from $Fe_{0.91}S$ to $Fe_{0.99}S$ [2].

The silicate, sulfide, and iron metal grains were mixed together in proportions similar to those found in LL-chondrites. The fraction of sulfide added was increased to allow easier investigation of the effects of metamorphism. The normative mineralogy of the experimental samples is compared to that of ordinary

Table 1
Composition of the silicate starting materials (wt%)

Oxide	Olivine	Quartz	Diopside	Anorthite	Feldspar	Experimental samples	LL-chondrite silicates[a,b]
MgO	49.0	–	26.1	–	–	38.6	30.6
FeO	10.0	–	–	–	–	7.6	17.3
SiO_2	41.0	100.0	55.6	43.4	68.4	48.7	46.6
CaO	–	–	17.7	20.0	1.4	1.6	1.9
Al_2O_3	–	–	–	37.0	18.7	2.5	2.6
K_2O	–	–	–	–	4.0	0.4	0.1
Na_2O	–	–	–	–	6.9	0.7	1.1
Total	100.00	100.00	99.4	100.4	99.4	100.1	100.2
Fraction[c]	0.755	0.070	0.060	0.017	0.098		

[a]Normative mineralogy from [5].
[b]Assuming a Mg# of 0.79 [11].
[c]Refers to weight fraction added to make the silicate mixture.

Table 2
Normative mineralogy of ordinary chondrites and experimental samples (wt%)

Mineral	Ordinary chondrites[a]			Experimental samples[b]
	H	L	LL	
Troilite	5.47	5.80	5.85	9.73
Metal	18.02	8.39	3.59	4.10
Olivine	35.04	44.83	51.92	47.84
Hypersthene	26.15	24.15	21.44	25.75
Diopside	4.11	4.97	5.34	3.47
Anorthite	1.70	1.59	1.55	2.21
Albite	7.30	8.07	8.11	4.90
Orthoclase	0.56	0.64	0.61	2.01
Ilmenite	0.23	0.24	0.25	0.00
Chromite	0.76	0.78	0.80	0.00
Apatite	0.65	0.54	0.54	0.00
Total	99.99	100.00	100.00	100.01

[a]Values from table 4 of [5].
[b]Calculated using the CIPW norm.

chondrites in Table 2. The goal of this work is to understand the mechanisms of sulfur transport in the primary system Fe–S during low temperature metamorphism of ordinary chondrites. Experiments designed to study the behavior of nickel during ordinary chondrite metamorphism are under way.

The mixture was pressed into pellets and placed in sealed, evacuated silica tubes. Each silica tube was attached to the end of a Pt–PtRh thermocouple and placed in the hot zone of a horizontal muffle tube furnace. The furnace was continuously flushed with high purity N_2 gas (99.999%) to minimize oxygen diffusion through the silica tube. Experiments were done at either 500°C or 900°C, representative peak temperatures experienced by type 3 and type 6 ordinary chondrites, respectively (see Table 3). The 900°C experiments were used to investigate a larger extent of reaction compared to the 500°C experiments. The furnace was brought up to the desired temperature within 30 min and held there for 2 weeks. After heating, the samples were cooled to room temperature and then removed from the silica tubes. The samples were mounted in epoxy and polished for analysis by optical and scanning electron microscopy, and electron microprobe. Electron microprobe analyses were made using the Washington University JEOL-733 electron microprobe and pyrite (FeS_2) was used as a primary standard.

Table 3
Metamorphic temperature of ordinary chondrites[a]

Metamorphic grade	Temperature range (°C)
3	400–600
4	600–700
5	700–750
6	750–950
7	> 950

[a]From [8].

3. Experimental results

All of our experimental samples show evidence of sulfur mobilization during heating. One line of evidence is the formation of sulfide crystals on the initially present iron metal grains. Fig. 1a is a back-scattered electron image of a metal grain in the sample heated at 500°C. Small sulfide crystals are observed in the pore spaces and along the outer edge of the metal grain. Sulfide formation in pore spaces penetrating the interior of metal grains indicates that sulfur vapor transport is the main mechanism for moving sulfur through the sample. The sulfide crystals are small (< 1 μm diameter) and are not abundant, suggesting only limited reaction in this sample.

Fig. 1b is a back-scattered electron image of two sulfide-rimmed metal grains in an experimental sample that reacted at 900°C. The extent of reaction in this sample is much larger than that seen in the sample that reacted at 500°C. The pore spaces initially present in the metal are now completely filled with sulfide. Sulfide rims surround the metal grains and incorporate nearby silicates. The assemblage on the left of Fig. 1b is partly surrounded by two distinct sulfide layers. The inner layer is composed of large sulfide crystals near the metal and the outer layer contains a continuous sulfide band that also surrounds several silicate grains. The thickness of the sulfide layers is variable. This is probably due to sulfide growth in initially porous regions near the metal. The sulfide grew rapidly in directions with a lot of pore space while only thin layers formed in regions where the metal was in contact with silicate grains. This is further evidence of vapor transport of sulfur through pore spaces.

Fig. 1c is a back-scattered electron image from the same experimental sample as shown in Fig. 1b (900°C). A thin sulfide rim is visible around the large metal grain at the left edge of the image. A small metal grain above this has been extensively sulfurized and a thick sulfide rim surrounds it. In addition, several smaller metal grains at the right edge of the image have been sulfurized to a lesser extent. The most interesting feature in this image is the thin band of sulfide that extends around neighboring silicate grains and connects the sulfide rims. The sulfide trail follows silicate grain boundaries and in several places encloses small silicate crystals. It is possible that these sulfide trails form by sulfurization of Fe-bearing silicates. However, if sulfurization of Fe from silicate took place, we should observe sulfide rims around silicate grains. Since the trails connect separate metal grains and Fe diffuses rapidly in sulfide [7], we suggest that the trails grow outward from the metal grains and that the Fe is supplied by diffusion from the metal through the sulfide trail.

Evidence of sulfur mobilization is also seen in the original sulfide grains added to the experimental samples. Fig. 2 shows a series of back-scattered electron images of the sulfides in our experimental samples. Fig. 2a is a pressed pellet assemblage before heating. The large grain in the center of the image is a 500 μm sulfide crystal. The sulfide grain has a hexagonal crystal structure and well defined crystal boundaries. Several cracks are visible throughout the grain but it is otherwise very compact with no apparent porosity. These are all common features of sulfides formed by gas–solid reactions [1–3]. The smaller white grains near the sulfide in Fig. 2a are iron metal and average about 50 μm in diameter. The metal grains are irregular and porous. The dark grains surrounding the metal and sulfide are silicates ranging in size from < 1 μm to 50 μm.

Fig. 2b is a back-scattered electron image of a sample heated at 500°C. The large sulfide in the center of this image shows evidence of sulfur loss as a result of heating. Sulfur was predominantly lost from high surface energy regions, such as the corners of the sulfide and along cracks and crystal edges. The corners are now rounded and uneven. The cracks have widened and there are no longer any sharp angles along the crystal boundaries. Numerous pores have formed throughout the sulfide.

Fig. 2c is a back-scattered electron image of a sample heated for 2 weeks at 900°C. A large sulfide grain is in the center of the image. The sulfide has been extensively corroded by heating. All of the evidence of sulfur loss seen in the previous sample (Fig. 2b), such as rounded corners, widening of cracks and crystal boundaries, and the formation of pores, are more developed in this sulfide. In addition, so much sulfur has been lost from this grain that iron metal has formed along its edge and large pores penetrate the grain.

Further evidence of sulfur loss from the sulfide grains is obtained from their composition. Fig. 3 shows the distribution of Fe/S ratios in the experimental sulfides as measured by electron microprobe. The composition of the unreacted sulfide grain (Fig. 2a) has a Gaussian distribution with Fe/S ratios that vary from 0.967 to 0.988 and have an average value of 0.976.

The compositions of the original sulfides heated at 500°C (Fig. 2b) are distributed bimodally, with one peak centered at $Fe/S = 0.995$ and the other at $Fe/S = 1.0025$. Since the Fe/S ratio of troilite cannot exceed unity, these data suggest that small grains of iron metal are present throughout these sulfides. The bimodal distribution reflects analyses of spots that contain metal versus those that do not. The average Fe/S ratio of these sulfides is 0.995, indicat-

Fig. 1. Back-scattered electron images of altered metal in our experimental samples. (a) An experimental sample heated at 500°C. Small sulfides have formed in the pore spaces and along the outer edge of the metal. Sulfide growth in regions devoid of silicates suggests that sulfur is transported as a vapor. (b) An experimental sample that reacted at 900°C. Often, two sulfide rims surround metal grains. In some areas there are several distinct sulfide crystals near the metal and a continuous band of sulfide beyond them. Notice how the sulfide layer will grow around and incorporate nearby silicate grains. (c) A back-scattered electron image from the same sample as (b). A well developed sulfide rim is seen around a metal grain and a sulfur trail connects the sulfide rims around several smaller metal grains. The trail follows silicate grain boundaries and in several places surrounds small silicate crystals. Sulfur trails such as these are also seen in ordinary chondrites.

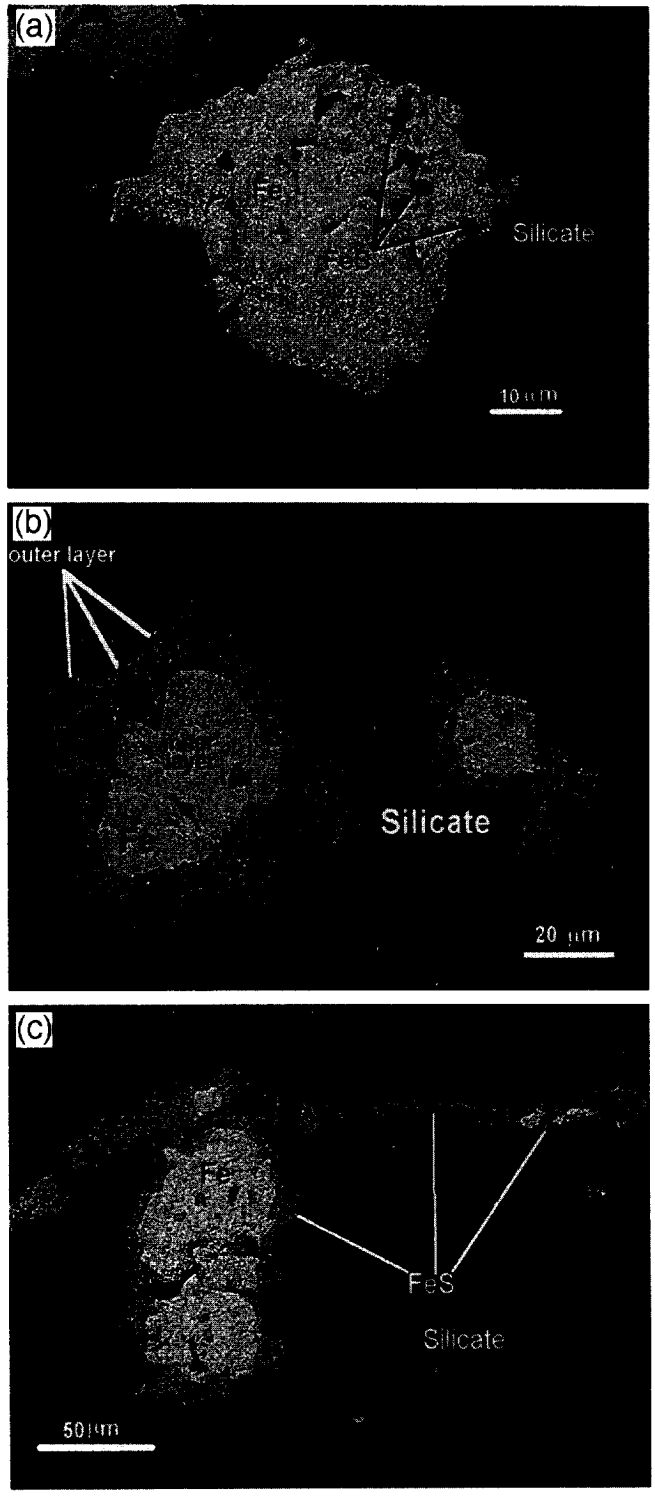
(a)
Fe
Silicate
10 μm
(b)
outer layer
Silicate
20 μm
(c)
Fe
FeS
Silicate
50 μm

ing that they have lost sulfur relative to the starting sulfide composition.

The compositions of the original sulfides heated at 900°C (Fig. 2c) have a Gaussian distribution. The compositional range is greater than that in the initial sulfide and the Fe/S ratios extend from 0.956 to 0.995. The average Fe/S ratio of these sulfides is slightly higher than that of the initial sulfides (0.980 vs. 0.976). However, large grains of iron metal have exsolved along the sulfide edges indicating that the bulk Fe/S ratios of the metal–sulfide assemblages are much higher than those of the initial sulfides.

The sulfide rims that formed on the metal grains at 900°C (Fig. 1b,c) are sulfur-rich compared to both the initial sulfide and the reacted sulfides in this sample. The Fe/S ratios of the newly formed sulfide rims range from 0.937 to 0.974 and have an average value of 0.961. Such sulfur-rich compositions imply that the sulfur fugacity present while these rims were forming was well above that in equilibrium with metal–troilite (see Fig. 4). The large variation in Fe/S ratios indicates that different local equilibria existed and global equilibrium was not reached.

4. Reaction mechanisms

Ordinary chondrites are divided into several metamorphic grades depending on the maximum temperature they experienced on their parent body. Table 3 shows the range of peak metamorphic temperatures estimated for each chondrite class [8]. Since sulfur is a moderately volatile element [9], it quickly responds to an increase in the temperature of chondrite parent bodies.

Thermal metamorphism drives isolated, non-equilibrium metal and sulfide grains towards equilibrium metal–sulfide assemblages. This approach to equilibrium is directly responsible for sulfur mobilization. However, equilibrium is a dynamic state in which the rate of sulfide formation in equal to that of sulfide decomposition. Thus, sulfur will continue to evaporate and recondense even after equilibrium is attained. There are three steps controlling the movement of sulfur during metamorphism of ordinary chondrites, each of which depends upon the metamorphic temperature. These are the supply, transport, and consumption of sulfur. Each of these processes is discussed in greater detail next.

4.1. Sulfur evaporation

Sulfur evaporates from sulfide grains and recondenses as sulfide rims on exposed metal. The driving force for this sulfur transport is the variation in sulfur fugacity throughout the experimental charge. Prior to heating, the sulfur fugacity in the sample is very small. When the temperature is increased the sulfur fugacity in equilibrium with a sulfide grain increases. As shown in Fig. 4, the sulfur fugacity in equilibrium with a sulfide grain (either pyrrhotite or troilite) is always greater than that in equilibrium with a metal–troilite assemblage. The equilibrium sulfur fugacity varies with the composition of the sulfide that is evaporating as well as with temperature. This variation is given as:

$$\ln f_{S_2,\text{pyrrhotite}} = 2\left(\ln(1 - X_{FeS}) + \ln\gamma_s - \frac{\Delta G_i^\circ}{RT}\right) \quad (2)$$

In this equation X_{FeS} is the Fe/S ratio in the pyrrhotite, ΔG_i° is the Gibbs free energy of pyrrhotite

Fig. 2. Back-scattered electron images showing the alteration of sulfides in our experiments (a) An experimental sample before it was heated. The large grain in the center is a sulfide crystal. Notice the hexagonal crystal structure and the well defined crystal boundaries. The crystal is cracked but not porous. The smaller white grains near the sulfide are iron metal whose shapes are irregular and contain much pore space. The dark material surrounding both the metal and sulfide are silicates. (b) A sulfide that has clearly been altered by heating at 500°C. There are no sharp angles on the crystal boundary. Cracks and crystal boundaries show evidence of loss of material. The cracks are larger and pores have started to form throughout the sulfide. (c) A sulfide that was heated for 2 weeks at 900°C. The sulfide has been extensively altered. The most obvious feature is the iron metal which has formed all along the edge of the sulfide crystal. The pores have become so large that some of them extend through the entire grain. The sulfide boundaries are rough and no sharp crystal edges are visible.

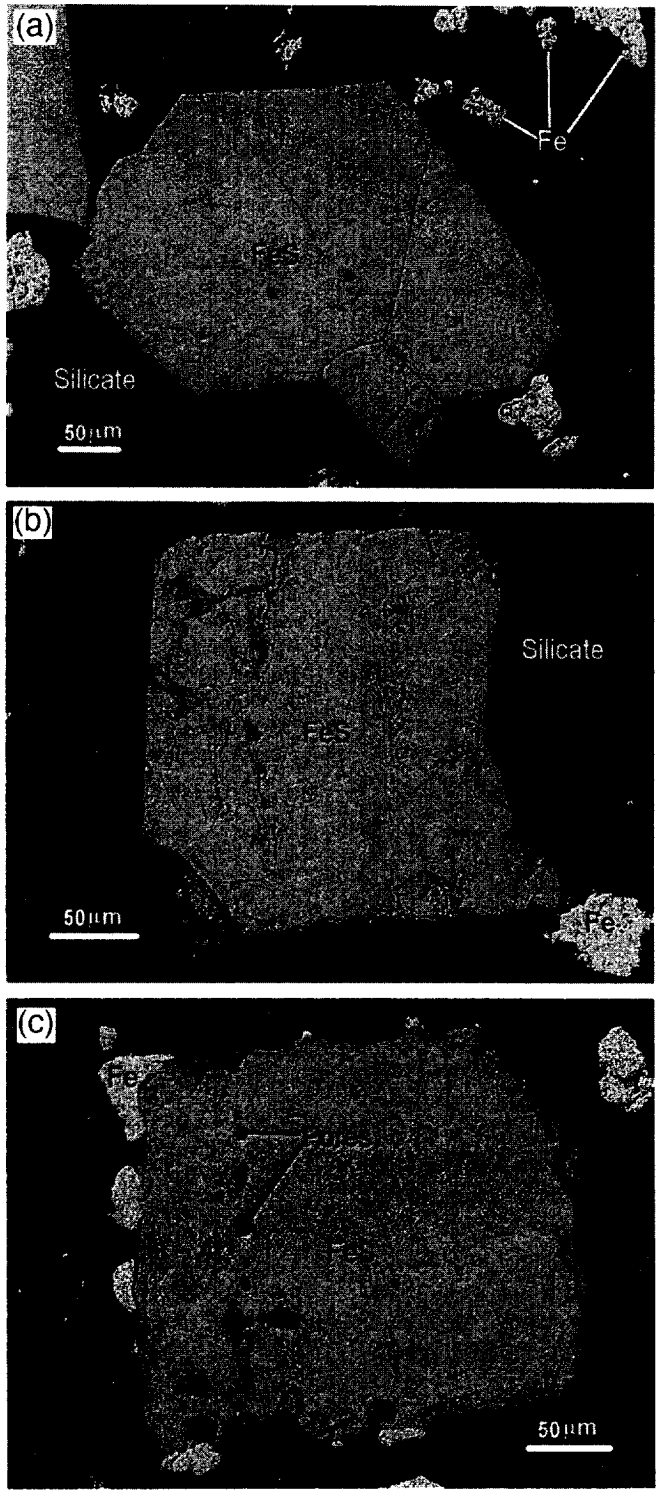
(a)
Fe
FeS
Silicate
50 μm
(b)
Silicate
FeS
50 μm
Fe
(c)
Fe
FeS
Fe
50 μm

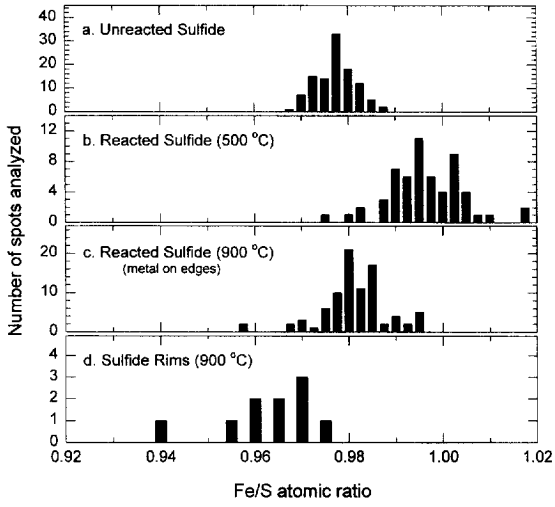

Fig. 3. Histograms of sulfide compositions given as Fe/S ratio. Fe/S ratios greater than 0.98 indicate troilite. (a) Composition of the unreacted sulfide grain shown in Fig. 2a. The Fe/S ratios display a gaussian distribution and range from 0.967 to 0.988 with an average value of 0.976. (b) The composition of the sulfide grain reacted at 500°C (Fig. 2b). The Fe/S ratios are distributed bimodally with one peak at Fe/S = 0.995 and the other at Fe/S = 1.0025. The latter peak is probably due to small grains of Fe metal contained within the sulfide. (c) The composition of the sulfide grain reacted at 900°C (Fig. 2c). The Fe/S ratios also display a gaussian distribution but have a wider range of compositions than the unreacted grain (0.956–0.995). The average Fe/S ratio is 0.980. This sulfide has grains of Fe metal along its edge, yielding a bulk Fe/S ratio above the starting composition. (d) The composition of sulfide rims that formed at 900°C (Fig. 1b,c). These sulfide are very sulfur-rich, with Fe/S varying from 0.937 to 0.974.

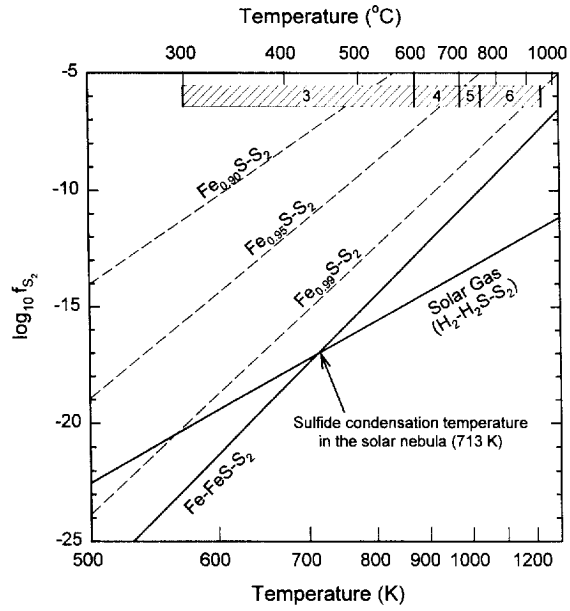

Fig. 4. A graph showing the variation of the sulfur fugacity with temperature and sulfide composition (Fe/S = 0.90, 0.95, and 0.99). The f_{S_2} curves for coexisting metal and troilite and a solar gas are also shown. In every case the f_{S_2} in equilibrium with a sulfide grain is higher than that in equilibrium with a metal–troilite assemblage. The range of metamorphic temperatures for each class of ordinary chondrites is shown by the bars at the top.

evaporation, R is the gas constant, T is temperature, and ln γ_S is the activity coefficient for S in pyrrhotite [10]. The sulfur fugacities in equilibrium with two different pyrrhotites ($Fe_{0.90}S$, $Fe_{0.95}S$), a troilite ($Fe_{0.99}S$), and coexisting iron metal and troilite (Fe–FeS) are plotted as a function of temperature in Fig. 4.

When the silicate–sulfide–metal mixture is heated, sulfur is lost from sulfide grains in the form of sulfur vapor. The sulfur fugacity above the sulfide is related to its initial composition. Sulfides release sulfur via the net reaction:

$$Fe_{1-x}S \rightarrow \underset{0.99}{0.99\,Fe_{1-x}S} + 0.005S_2 \qquad (3)$$

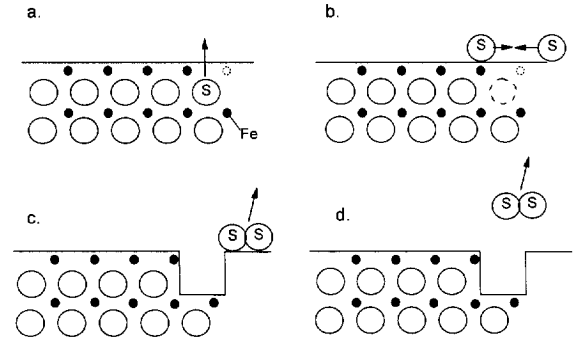

Fig. 5. A cartoon showing the loss of sulfur from a sulfide grain. The large circles represent sulfur atoms. The small dots represent iron atoms. A vacancy in the solid is represented by a dashed circle. (a) A sulfur atom is removed from the crystal lattice and becomes an adsorbed atom on the crystal surface. (b) Two adsorbed sulfur atoms react to form an S_2 molecule. (c) A void is formed in the crystal due to the loss of the sulfur atom. The S_2 molecule desorbs from the crystal surface. (d) The final assemblage is a more iron-rich sulfide and a gaseous S_2 molecule.

which occurs by a series of elementary reactions such as:

$$Fe_{1-x}S + \square \rightarrow \underbrace{0.99\,Fe_{1-x}S}_{0.99} + 0.01\,S(ad) \quad (4)$$

$$2S(ad) \rightarrow S_2(ad) \quad (5)$$

$$S_2(ad) \rightarrow S_2(gas) + \square \quad (6)$$

In these equations $\square$ represents a vacant surface site on the sulfide, and (ad) refers to a species adsorbed on the surface of the sulfide.

Fig. 5a shows the loss of a sulfur atom from the sulfide crystal lattice. The sulfur atom breaks free of the bond with iron and becomes a single atom adsorbed on the crystal surface. Fig. 5b shows two sulfur atoms that have been liberated from the crystal lattice joining together to form an adsorbed S_2 molecule. In Fig. 5c the adsorbed S_2 molecule desorbs from the surface of the sulfide leaving behind a vacant surface site. Fig. 5d shows the final result of sulfur loss. The sulfide crystal is now smaller and more iron rich while the S_2 molecule is in the gas phase and moving away from the sulfide. This series

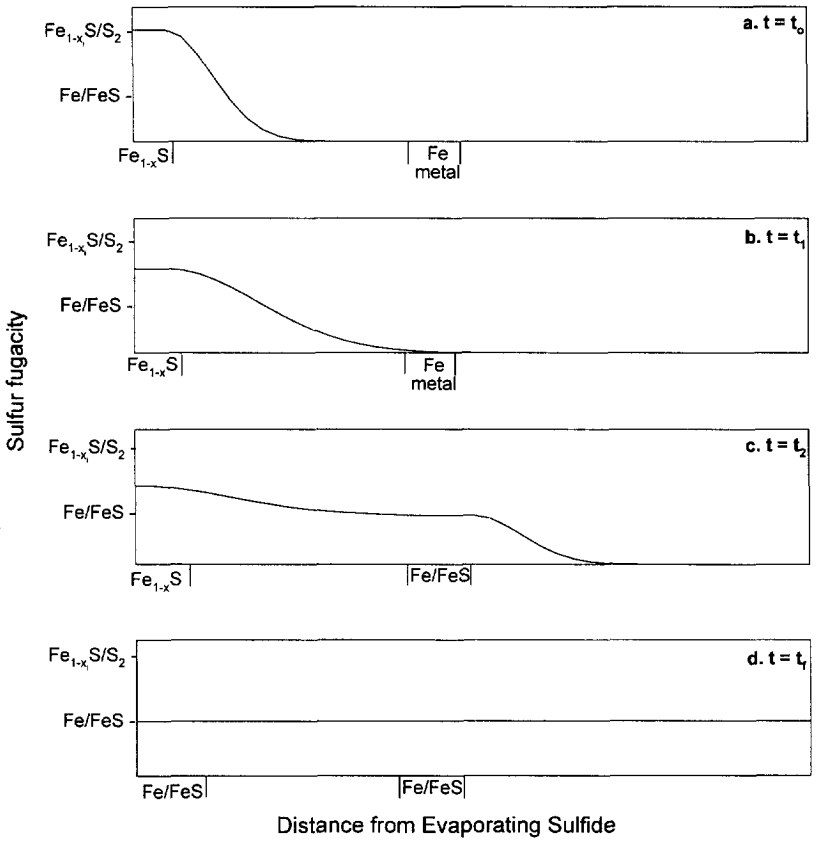

Fig. 6. Cartoons showing the f_{S_2} (y axis) as a function of distance from an evaporating sulfide (x axis). Two values for f_{S_2} are labeled on the y axis. The label $Fe_{1-x}S/S_2$ represents the sulfur fugacity in equilibrium with the initial pyrrhotite composition while Fe/FeS represents the sulfur fugacity in equilibrium with coexisting iron metal and troilite. (a) The f_{S_2} is described by a diffusion profile away from the grain. The f_{S_2} near the grain is determined by $Fe_{1-x}S/S_2$ equilibrium. An iron metal grain is present some distance away from the sulfide. (b) The sulfur fugacity is still described by a diffusion profile. Loss of sulfur has caused the Fe/S ratio in the sulfide to increase, leading to a lower equilibrium sulfur fugacity near the sulfide. (c) The metal grain begins to sulfurize and the sulfur fugacity is fixed at Fe/FeS at the edge of the metal. A diffusion profile still describes the sulfur fugacity in regions between the sulfide and the iron metal but the sulfur fugacity beyond the metal grain is at Fe/FeS or less. (d) Equilibrium is reached throughout the sample. The sulfur fugacity is in equilibrium with coexisting metal and sulfide and is uniform throughout the sample.

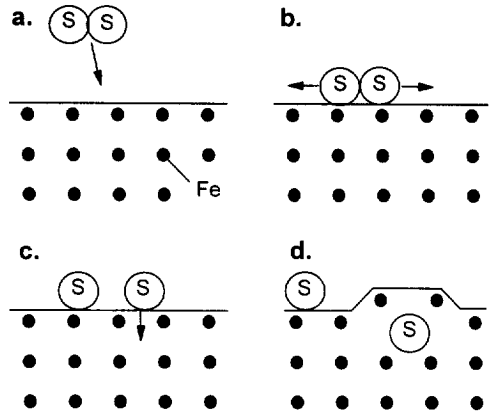

Fig. 7. A cartoon showing elementary chemical reactions for sulfur condensation on an iron grain. The large circles represent sulfur atoms. The small circles represent iron atoms. (a) An S_2 molecule is adsorbed on the metal surface. (b) The S_2 molecule dissociates to form two sulfur atoms. (c) One of the sulfur atoms reacts with an iron atom to form iron sulfide. (d) The final assemblage.

of sulfide decomposition reactions will proceed until the f_{S_2} near the sulfide reaches the S_2 vapor pressure in equilibrium with the sulfide.

4.2. Sulfur transport

Sulfur diffuses along sulfur vapor concentration gradients that are established throughout the sample between evaporating sulfide grains ($Fe_{1-x}S$–S_2 equilibrium) and sulfide rims condensed on metal (Fe–FeS–S_2 equilibrium). The transport of sulfur vapor prevents the equilibrium sulfur fugacity from being reached near the sulfide. Thus, throughout metamorphism sulfides continuously evaporate to replace sulfur vapor that diffused away and condensed on metal. Eventually enough sulfur is lost and iron metal exsolves from the sulfide and the sulfur fugacity near the original sulfide is also buffered by Fe–FeS equilibrium.

The variation in the sulfur fugacity with distance from the evaporating sulfide can be described by a simple diffusion profile. A simplified model of the evolution of sulfur fugacity with distance from an evaporating sulfide is shown in Fig. 6. The y axis in Fig. 6 qualitatively displays the sulfur fugacity in equilibrium with pyrrhotite ($Fe_{1-x}S$) and coexisting metal–troilite. As illustrated in Fig. 4, the f_{S_2} increases with decreasing Fe/S ratio in the sulfide. Thus, the f_{S_2} over pyrrhotite is larger than the f_{S_2} over coexisting metal–troilite. The x axis in Fig. 6 represents the distance from the evaporating sulfide grain. One location at which a sulfide grain forms from an initially present metal grain is also shown. Fig. 6 is a series of 'snapshots' at four different times, ranging from an initial time, t_0, to a final time, t_f, of the f_{S_2} profile as a function of distance in a sample heated at constant temperature.

Fig. 6a shows the variation in f_{S_2} at the initial time (t_0). There is a steep variation in f_{S_2} with distance from the evaporating sulfide grain. The f_{S_2} in the neighborhood of the grain is equal to that in equilibrium with the sulfide. Chemical potential and pressure gradients lead to S_2 diffusion away from the evaporating grain which is being depleted in sulfur.

Fig. 6b shows the f_{S_2} variation at an intermediate time (t_1). As the sulfide grain continues losing sulfur it becomes more Fe-rich and the f_{S_2} in the neighborhood of the grain decreases accordingly. The variation in f_{S_2} with distance is less steep and the f_{S_2} is higher at greater distances from the evaporating grain. Sulfur vapor reaches an Fe metal grain in the sample, but does not yet react with it since the f_{S_2} at the metal grain is still less than the f_{S_2} over coexisting metal–troilite.

Fig. 6c shows the change in the f_{S_2} variation when FeS first begins to form on a metal grain (t_3). The composition of the evaporating sulfide is approaching FeS and the f_{S_2} at this location continues to decrease. The f_{S_2} continues to increase at greater distances from the evaporating sulfide grain and has

Fig. 8. Reflected light images of metal–sulfide assemblages in ALH-76004. The field of view in all of the photographs is 500 μm. (a) A sulfide rim that closely resembles those seen in the experimental samples surrounds a metal grain. The sulfides extend around and incorporate nearby silicate grains. Two distinct sulfide rims are present in several places as well (photo from [3]). (b) This image shows two sulfide-rimmed metal grains connected by a thin trail of iron sulfide. Such features were also observed in the experimental samples. (c) This sulfide-rimmed metal grain shows evidence of sulfur loss similar to that seen from the sulfides in the experimental samples. A thin rim of iron metal partially surrounds the sulfide. In addition, the sulfide is very porous and contains several wide cracks.

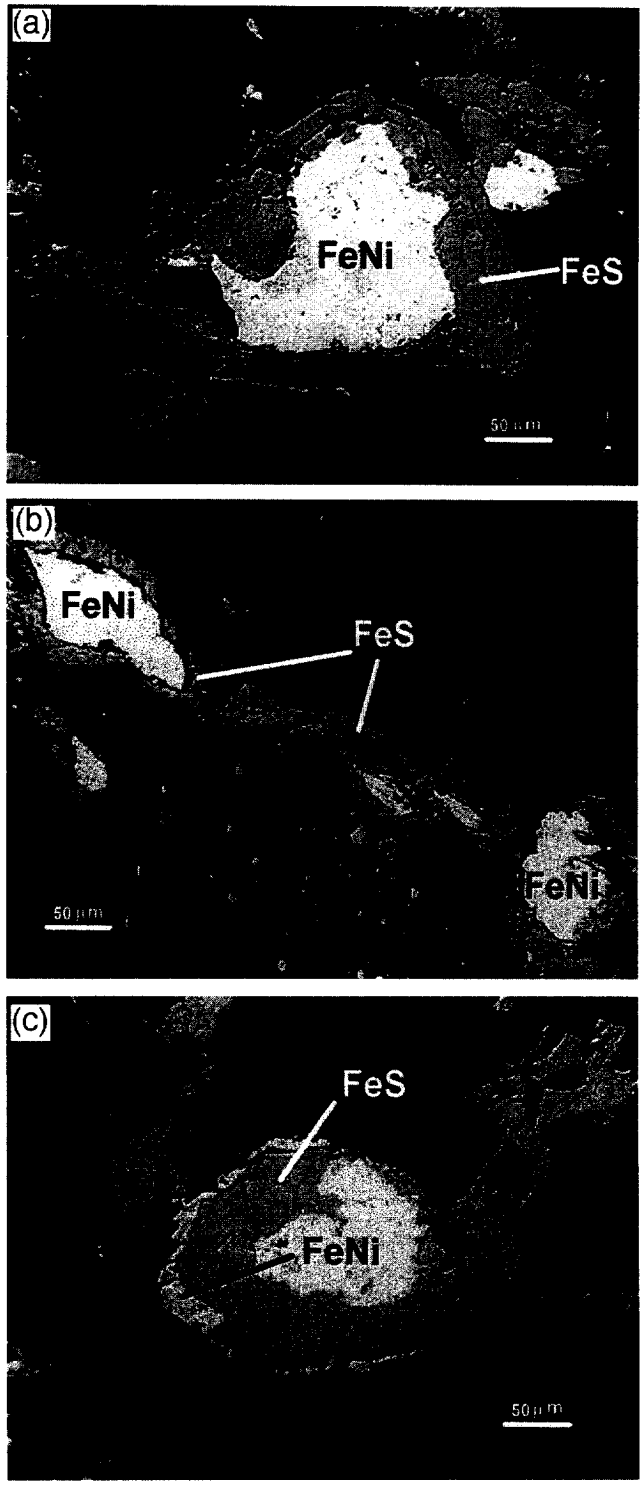
(a)
FeNi
FeS
50 μm
(b)
FeNi
FeS
FeNi
50 μm
(c)
FeS
FeNi
50 μm

reached the f_{S_2} in equilibrium with coexisting metal–troilite at the location of the Fe metal grain.

Fig. 6d shows the sulfur fugacity in the sample when equilibrium is reached (t_f). The f_{S_2} is the same throughout the sample. The initial sulfide grain has converted into Fe and FeS. The dynamic equilibrium between the two metal–troilite assemblages leads to continuous sulfur evaporation, transport, and recondensation. However, as demonstrated by the sulfide compositions, equilibrium was not reached in our samples.

4.3. Sulfur condensation

Sulfide will condense on a metal grain when the sulfur fugacity is at or above that in equilibrium with coexisting metal and troilite. From the above arguments we know that the sulfur fugacity in equilibrium with the evaporating sulfides is above that for coexisting metal and troilite. In addition, the sulfur fugacity decreases with distance from the evaporating sulfide. This implies that at some distance away from the evaporating sulfide grain the sulfur fugacity will be equal to or greater than that in equilibrium with metal–troilite. If there is a metal grain present at this location then the sulfur vapor condenses on the metal grain to form a sulfide rim.

Sulfide formation on the iron metal grains in this system occurs via the net reaction:

$$(1 - x)\,Fe + 1/2S_2 \rightarrow Fe_{1-x}S \quad (7)$$

This reaction can be broken up into a series of elementary chemical reactions such as:

$$S_2(gas) + \square \rightarrow S_2(ad) \quad (8)$$

$$S_2(ad) \rightarrow 2\,S(ad) \quad (9)$$

$$(1 - x)Fe + S(ad) \rightarrow Fe_{1-x}S + \square \quad (10)$$

This series of reactions is shown schematically in Fig. 7.

In Fig. 7a an S_2 molecule is adsorbed on the metal surface. Fig. 7b shows the dissociation of the S_2 molecule into two sulfur atoms. One of the sulfur atoms reacts with an iron atom to form a small region of FeS in Fig. 7c. Since FeS has a larger molar volume than Fe, the sulfide extends above the original sulfide surface, as shown in Fig. 7d. Sulfide formation on the iron metal grains will continue until equilibrium between the metal–sulfide assemblages and the gas is reached.

5. Comparison with meteoritic metal–sulfide assemblages

The morphologies of the metal–sulfide assemblages in the experimental samples are strikingly similar to those found in low metamorphic grade chondrites. Fig. 8a is a reflected light photomicrograph of a metal–sulfide assemblage from the LL3 unequilibrated ordinary chondrite ALH-76004. The sulfide layers surrounding the metal grain resemble those formed by sulfurization of iron or iron–nickel alloys in H_2–H_2S gas mixtures. However, the meteoritic sulfide does not contain a nickel concentration gradient and is thus different to the monosulfide solid solution formed by the reaction of H_2S with FeNi metal, as expected for pristine nebular sulfides [1]. Therefore, we argue that the composition of the sulfide rim in Fig. 8a was most likely established during a heating event on the chondrite parent body [1]. This argument is supported by similarities between the metal–sulfide assemblages in ALH-76004 and the sulfide-rimmed metal grains formed in our metamorphism experiments. In both the meteoritic and the experimental metal–sulfide assemblages the metal grains are surrounded by at least two distinct sulfide layers which incorporate neighboring grains (Fig. 1b,c and Fig. 7a,b). The thickness of the sulfide rims vary, with the widest rims present in regions devoid of silicates.

Sulfide trails connecting several sulfide-rimmed metal grains were observed in the experimental samples (Fig. 1c). These features are also seen in ordinary chondrites. Fig. 8b shows analogous features in ALH-76004. In this figure there are two sulfide-rimmed metal grains of roughly equivalent size. A thin trail of sulfide connects the two assemblages. This is further evidence that metamorphism of the LL-chondrite parent body caused extensive sulfur mobilization.

Fig. 8c is a photomicrograph of another sulfide grain from ALH-76004. In this case, a band of iron metal is present along the outer edge of the sulfide. In addition, the sulfide is porous and contains wide

cracks. These features are also observed in the sulfide grains in our experiments (Fig. 2c) as a result of sulfur loss due to heating. Thus, the features indicative of sulfur mobilization in our experimental samples are present in the LL3 chondrite ALH-76004. Several of these features are unique to the metamorphic process including: the growth of sulfide layers around neighboring silicate grains, the presence of thin sulfide trails, and the formation of iron metal at the outer edge of sulfide crystals. We conclude that significant sulfur mobilization occurred on the parent body of ALH-76004 as a result of thermal metamorphism.

6. Summary

We report the first results of an experimental study of sulfide chemistry during metamorphism of the LL-chondrite parent body. Our experiments correspond to metamorphic temperatures experienced by type 3 and type 6 ordinary chondrites. Sulfide grains formed on metal after only 2 weeks of reaction at 500°C while extensive sulfide rims formed after 2 weeks at 900°C. The morphologies of the sulfide rims suggest that sulfur is transported through the silicate matrix as a vapor, most likely S_2. The original sulfide grains, which are compact and have well defined crystal boundaries, become extensively altered within short time periods. Sulfide grain boundaries, corners, and cracks in the crystals show loss of sulfur. Large pores form within the sulfide grains and, after extensive reaction, iron metal appears along the sulfide grain boundaries. The experimental metal–sulfide assemblages bear a striking resemblance to metal–sulfide assemblages seen in the LL3 chondrite ALH-76004. Our work shows that sulfur mobilization and alteration of nebular sulfides probably occurred in even the lowest metamorphic grade ordinary chondrites. It is uncertain whether information about the solar nebula recorded in nebular sulfide condensates can survive this process.

Acknowledgements

This work was supported by NASA grant NAGW-3070. We thank the NIPR in Tokyo for use of the ALH-76004 section and the Feldspar Corporation for the feldspar used in these experiments. *[CL]*

References

[1] D.S. Lauretta, D.T. Kremser, B. Fegley Jr., A comparative study of experimental and meteoritic metal–sulfide assemblages, in: Proc. NIPR Symp. on Antarctic Meteorites 9, 1996, pp. 97–110.

[2] D.S. Lauretta, D.T. Kremser, B. Fegley Jr., The rate of iron sulfide formation in the solar nebula, Icarus 122 (1996) 288–315.

[3] D.S. Lauretta, B. Fegley Jr., K. Lodders, D.T. Kremser, The kinetics and mechanism of iron sulfide formation in the solar nebula, in: Proc. NIPR Symp. on Antarctic Meteorites 9, 1996, pp. 111–126.

[4] J.A. Wood, Chondrites: Their metallic minerals, thermal histories, and parent planets, Icarus 6 (1967) 1–49.

[5] H.Y. McSween Jr., M.E. Bennett III, The mineralogy of ordinary chondrites and implications for asteroid spectrophotometry, Icarus 90 (1991) 107–116.

[6] E.T. Turkdogan, Iron–sulfur system Part I: Growth rate of ferrous sulfide on iron and diffusivities of iron in ferrous sulfide, Trans. AIME 242 (1968) 1665–1672.

[7] R.H. Condit, R.R. Hobbins, C.E. Birchenall, Self-diffusion of iron and sulfur in ferrous sulfide, Oxid. Met. 8 (1974) 409–455.

[8] R.T. Dodd, Meteorites, A Petrologic–Chemical Synthesis, Cambridge University Press, Cambridge, UK, 1981, 368 pp.

[9] J.W. Larimer, The cosmochemical classification of the elements, in: J.F. Kerridge, M.S. Matthews (Eds.), Meteorites and the Early Solar System, University of Arizona Press, Tucson, 1988, pp. 375–389.

[10] E. Froese, A.E. Gunter, A note on the pyrrhotite–sulfur vapor equilibrium, Econ. Geol. 71 (1976) 1589–1594.

[11] J.T. Wasson, G.W. Kallemeyn, Compositions of chondrites, Philos. Trans. R. Soc. London Ser. A 325 (1988) 535–544.